Analysis and Optimization of a 2-D Magnet Array with Hexagon Magnet

G. Liu, Y. Zhou, R. Zhou, W. Ming, and L. Huo

School of Mechanical Science and Engineering,
Huazhong University of Science and Technology, Wuhan 430074, China
lgd5401@gmail.com, yfzhou@mail.hust.edu.cn, rougangzhou@hust.edu.cn, mingwuyi81@gmail.com, liganghuo@126.com

Abstract ─ This paper introduces the hexagon permanent magnets, which are in *x*- or *y*- axis magnetized directions to the 2-D permanent magnet array for planar motor. Through the scalar magnetic potential equation, finite element method and effective amplitudes, the harmonic and analytical models are derived and verified. The reduction of the higher harmonics of *z*-component of the magnetic flux density with hexagon magnets is verified. Low higher harmonics of *z*-component of the magnetic flux density with hexagon magnets is optimized by the genetic algorithm. Comparing with the 2-D Halbach magnet arrays, the new magnet array has larger *z*-component of the magnetic flux density and smaller higher harmonics of *z*-component of the magnetic flux density, which can reduce the force ripples of planar motor.

Index Terms ─ Effective amplitude, force ripples, genetic algorithm, hexagon magnet, magnet array, and planar motor.

I. INTRODUCTION

In many industrial apparatus, like pick-and-place machines, lithography and inspection systems, objects are positioned and moved in a horizontal plane [1-10]. The magnetically levitated planar motors with 2-D permanent magnet array, which have the advantages of large range planar motion, simple structure, high speed, and high precision, have received increasing attention. Until now some types of planar motors, which can move freely in any directions in the plane have been proposed.

Cho et al. [2] proposed a magnet array for planar motor with compact structure to obtain high magnetic flux density. The magnetic field was obtained by using the scalar magnetic potential. But the harmonic model is too complex to apply in real time control. To deal with this problem, Cho et al. [3] substitute a 2-D sinusoidal wave with flux density exponentially decreasing across the air-gap length for the flux density distribution. In contrast with Cho et al, Jansen et al. [4, 5] proposed a new type of 2-D Halbach magnet array, derived an analytical model by taking the first harmonic of the magnetic flux density and optimized the 2-D Halbach magnet array by maximizing the magnetic flux density per unit of moving-part for low power dissipation. However, the higher harmonics of the magnet array is high, which is usually a main reason for the force ripples in planar motor [6]. To get a magnet array with high magnetic flux density and low higher harmonics, W. Min et al. [6] proposed a 2-D Halbach array with 4 segments per pole and adopting the genetic algorithm (GA) to minimize the higher harmonics. Y. Zhang [7] and L. Huang et al. [8] investigated different 1-D magnet array topologies and found the trapezoidal permanent magnet structures had a reduced number of high harmonic components. J. Peng et al. [9] proposed a 2-D Halbach array by using trapezoidal magnets. The trapezoidal magnets, which have a 45° magnetized direction are used to reduce the higher harmonics and increase the intensity of the magnetic field. The analytical model is derived by taking the amplitude of the magnetic flux density as the effective amplitude. The genetic algorithm is also used to minimize the higher harmonics.

Submitted On: March 15, 2013
Accepted On: Sept. 29, 2013

The new 2-D magnet array proposed by this paper has the features of compact structure, without magnets of 45° magnetized direction and using hexagon magnets. The hexagon magnets are used to reduce higher harmonics and increase the intensity of the magnetic field. The harmonic model of the magnetic flux density for the new array is derived by Fourier series and the scalar magnetic potential [11], and verified by finite element method. The analytical model is derived by the effective amplitude. The genetic algorithm is used to minimize the higher harmonics in *z*-component of the magnetic flux density. Finally, the new array is compared with the 2-D Halbach array used by Jansen [4].

II. ANALYSIS OF MAGNETIC FLUX DENSITY

A. Analytical model

Figure 1 shows the magnet array with top view and cut-view. The magnetized direction of the magnets is denoted by the arrows from S-pole to N-pole, and S means the direction towards the paper and N means out of paper. The hexagon magnets are in the horizontal directions. The magnet array modeled as infinitely large with Fourier series by neglecting end effects. The residual magnetization vector of the magnet array with the permanent magnets can be expressed as,

$$\vec{M} = M_x \hat{x} + M_y y + M_z \hat{z}. \tag{1}$$

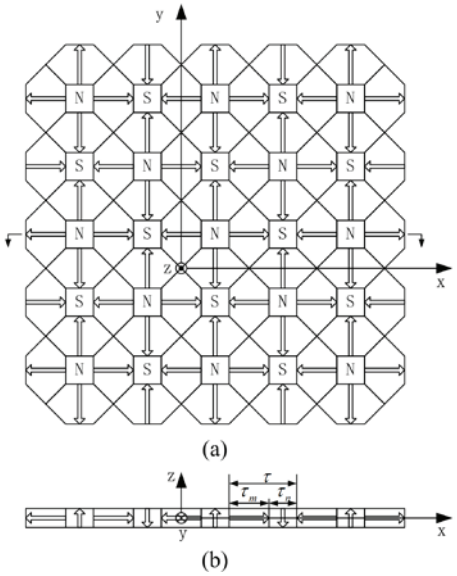

Fig. 1. Magnet array; (a) top and (b) cut-views.

Figure 2 shows the M_x projection distribution of the hexagon magnets. The projection distribution is derived by using Fourier series. The expression of M_x is,

$$\begin{aligned} M_x &= PMX_y \cdot PMX_x \cdot M \\ &= M\sum_{k=1}^{\infty}\sum_{l=1}^{\infty} a_{xk} b_{xl} \cos(k\omega x)\sin(l\omega y) \end{aligned}, \tag{2}$$

where $M=B_r/\mu_0$, $\omega=\pi/\tau$, k and l are the harmonic numbers for the x- and y-direction, respectively. While a_{xk} and b_{xl} are the projection distribution coefficients, τ is the pole pitch, τ_m is the length of the side of the magnets, which are magnetized in z-direction, and

$$a_{xk} = -\frac{4}{k\pi}\sin\frac{k\pi}{2}\cos\frac{k\omega\tau_m}{2} \tag{3}$$

$$b_{xl} = \frac{4}{l\pi}\sin^2\frac{l\pi}{2}\cos\big(l\omega v(x)\big). \tag{4}$$

The $v(x)$ is a function of the variable x due to the shape of hexagon magnet [9]. The distribution of variable x in a period with thick line is shown in Fig. 2 and expressed as

$$v(x) = \begin{cases} x+\tau & -\tau \le x < -0.5\tau \\ -x & -0.5\tau \le x < 0 \\ x & 0 \le x < 0.5\tau \\ -x+\tau & 0.5\tau \le x \le \tau \end{cases}. \tag{5}$$

The expression of cos ($l\omega v(x)$) is obtained using equation (5)

$$\begin{aligned} \cos\big(l\omega v(x)\big) &= \begin{cases} -\cos(u\omega x) & -\tau \le x < -0.5\tau \\ \cos(u\omega x) & -0.5\tau \le x < 0 \\ \cos(u\omega x) & 0 \le x < 0.5\tau \\ -\cos(u\omega x) & 0.5\tau \le x \le \tau \end{cases} \\ &= \lambda_{v(x)}\cos(u\omega x) \end{aligned}, \tag{6}$$

where $\lambda_{v(x)}$ is distribution coefficient. Figure 3 shows the distribution of $\lambda_{v(x)}$, and the expression is obtained by Fourier series

$$\lambda_{v(x)} = \sum_{u=1}^{\infty}\frac{4}{u\pi}\sin\frac{u\pi}{2}\cos(u\omega x), \tag{7}$$

where u is harmonic number.

M_y can be constructed by interchanging the variables x and y in the function of M_x. The M_z projection distribution of the cubic magnets is obtained by conventional approach with Fourier series and not list. The expressions of the residual magnetization vector of this array are,

$$M_x = -M\sum_{k=1}^{\infty}\sum_{l=1}^{\infty}\sum_{u=1}^{\infty} g(k)C\sin(l\omega y)\left(\cos(e_1\omega x) + \cos(e_2\omega x) + \cos(e_3\omega x) + \cos(e_4\omega x)\right) \quad (8)$$

$$M_y = -M\sum_{k=1}^{\infty}\sum_{l=1}^{\infty}\sum_{u=1}^{\infty} Cg(l)\sin(k\omega x)\left(\cos(e_5\omega y) + \cos(e_6\omega y) + \cos(e_7\omega y) + \cos(e_8\omega y)\right) \quad (9)$$

$$M_z = M\sum_{k=1}^{\infty}\sum_{l=1}^{\infty} a(k)a(l)\sin(k\omega x)\sin(l\omega y), \quad (10)$$

where τ_n is the length of the side of the hexagon magnets, and

$$C = \frac{16}{klu\pi^3}\sin^2\frac{k\pi}{2}\sin^2\frac{l\pi}{2}\sin\frac{u\pi}{2} \quad (11)$$

$$g(k) = \sin\frac{k\omega\tau_n}{2}, \quad (12)$$

$$a(k) = \frac{4}{k\pi}\sin^2\frac{k\pi}{2}\cos\frac{k\omega\tau_n}{2}, \quad (13)$$

$$e_1 = k + l + u, \quad (14)$$

$$e_2 = k + l - u, \quad (15)$$

$$e_3 = k - l + u, \quad (16)$$

$$e_4 = k - l - u, \quad (17)$$

$$e_5 = l + k + u, \quad (18)$$

$$e_6 = l + k - u, \quad (19)$$

$$e_7 = l - k + u, \quad (20)$$

$$e_8 = l - k - u. \quad (21)$$

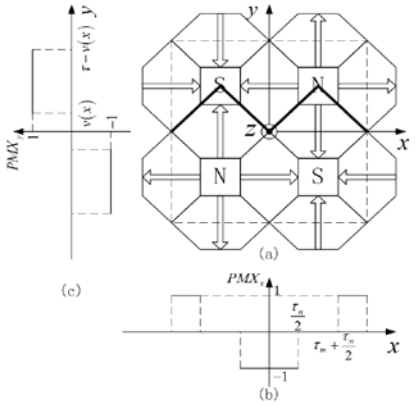

Fig. 2. M_x projection distribution of the hexagon magnets; (a) magnet array, (b) x-directoin, and (c) y-direction.

B. Governing and solving equation

To derive the magnetic flux density of the magnet array, the 3-D space is divided into three regions [11] of which a cross section is shown in Fig. 4. Regions 1 and 3 are in air. The permanent magnets in region 2 are located in between $m_b \le z \le m_t$. The assumption of air in the magnet array is not existed due to the compact structure.

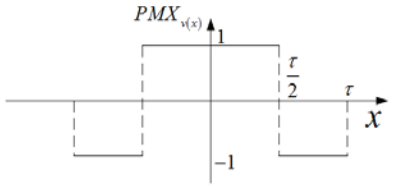

Fig. 3. Distribution of $\lambda_{v(x)}$.

The scalar magnetic potential equation is applied to this problem because there is no current. In regions 1 and 3, the next equations apply (only the equations for region 1 are shown),

$$\vec{H}_1 = -\nabla\Psi_1 \quad (22)$$

$$\nabla\times\vec{H}_1 = 0, \quad (23)$$

$$\vec{B}_1 = \mu_0\vec{H}_1, \quad (24)$$

$$\nabla\cdot\vec{B}_1 = 0, \quad (25)$$

where $\vec{B}_1$ is the magnetic flux density, $\vec{H}_1$ is the magnetic field strength, Ψ_1 is the scalar potential. In region 2,

$$\vec{H}_2 = -\nabla\Psi_2 \quad (26)$$

$$\nabla\times\vec{H}_2 = 0, \quad (27)$$

$$\vec{B}_2 = \mu_0\mu_r\vec{H}_2 + \mu_0\vec{M}, \quad (28)$$

$$\nabla\cdot\vec{B}_2 = 0, \quad (29)$$

where μ_r is the relative permeability. After the substitution of the scalar potential in equations (22) to (25) and equations (26) to (29), respectively, the following equations are obtained,

$$\nabla^2\Psi_1 = 0 \quad (30)$$

$$\nabla^2\Psi_2 = \nabla\cdot\frac{\vec{M}}{\mu_r} = \frac{M}{\mu_r}\times \left(\sum_{k=1}^{\infty}\sum_{l=1}^{\infty}\sum_{u=1}^{\infty} g(k)C\sin(l\omega y)\sum_{i=1}^{4} e_i\omega\sin(e_i\omega x) + \sum_{k=1}^{\infty}\sum_{l=1}^{\infty}\sum_{u=1}^{\infty} g(l)C\sin(k\omega x)\sum_{j=5}^{8} e_j\omega\sin(e_j\omega x)\right), \quad (31)$$

$$\nabla^2\Psi_3 = 0. \quad (32)$$

At infinite distance from the magnet array,

$$\Psi_1(z=\infty) = 0 \quad (33)$$

$$\Psi_3(z=-\infty) = 0. \quad (34)$$

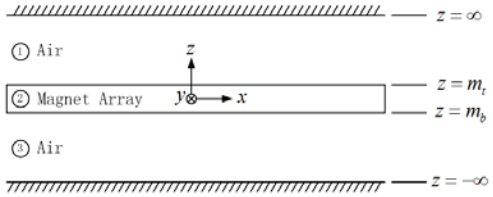

Fig. 4. Space divided into three regions.

The following boundary conditions apply on the interface between the magnets and the air (see also Fig. 4),

$$H_{1x}\left(z=m_t\right)=H_{2x}\left(z=m_t\right) \tag{35}$$

$$H_{1y}\left(z=m_t\right)=H_{2y}\left(z=m_t\right), \tag{36}$$

$$B_{1z}\left(z=m_t\right)=B_{2z}\left(z=m_t\right), \tag{37}$$

$$H_{2x}\left(z=m_b\right)=H_{3x}\left(z=m_b\right), \tag{38}$$

$$H_{2y}\left(z=m_b\right)=H_{3y}\left(z=m_b\right), \tag{39}$$

$$B_{2z}\left(z=m_b\right)=B_{3z}\left(z=m_b\right). \tag{40}$$

where m_t, m_b is the height of the magnet array.

The method of separation of variables is used to solve the Laplace equations. A solution of the scalar potential is substituted,

$$\begin{aligned}\Psi=&\sum_{k=1}^{\infty}\sum_{l=1}^{\infty}\sum_{u=1}^{\infty}\sin\left(l\omega y\right)\sum_{i=1}^{4}Z_i\left(z\right)\sin\left(e_i\omega x\right)\\&+\sum_{k=1}^{\infty}\sum_{l=1}^{\infty}\sum_{u=1}^{\infty}\sin\left(k\omega x\right)\sum_{i=5}^{8}Z_i\left(z\right)\sin\left(e_i\omega x\right)\\&+\sum_{k=1}^{\infty}\sum_{l=1}^{\infty}Z_0\left(z\right)\sin\left(k\omega x\right)\sin\left(l\omega y\right).\end{aligned} \tag{41}$$

In regions 1 and 3, substitution of equation (41) into equation (30) results in,

$$\begin{aligned}&\sum_{k=1}^{\infty}\sum_{l=1}^{\infty}\sum_{u=1}^{\infty}\sin\left(l\omega y\right)\sum_{i=1}^{4}\left(\frac{d^2Z_i\left(z\right)}{dz^2}-\lambda_i^{\,2}Z_i\left(z\right)\right)\sin\left(e_i\omega x\right)+\\&\sum_{k=1}^{\infty}\sum_{l=1}^{\infty}\sum_{u=1}^{\infty}\sin\left(k\omega x\right)\sum_{i=5}^{8}\left(\frac{d^2Z_i\left(z\right)}{dz^2}-\lambda_i^{\,2}Z_i\left(z\right)\right)\sin\left(e_i\omega y\right)+\\&\sum_{k=1}^{\infty}\sum_{l=1}^{\infty}\sin\left(k\omega x\right)\sin\left(l\omega y\right)\left(\frac{d^2Z_0\left(z\right)}{dz^2}-\lambda_0^{\,2}Z_0\left(z\right)\right)=0\end{aligned} \tag{42}$$

where

$$\lambda_1=\sqrt{\left(l\omega\right)^2+\left(e_1\omega\right)^2}, \tag{43}$$

$$\lambda_2=\sqrt{\left(l\omega\right)^2+\left(e_2\omega\right)^2}, \tag{44}$$

$$\lambda_3=\sqrt{\left(l\omega\right)^2+\left(e_3\omega\right)^2}, \tag{45}$$

$$\lambda_4=\sqrt{\left(l\omega\right)^2+\left(e_4\omega\right)^2}, \tag{46}$$

$$\lambda_5=\sqrt{\left(k\omega\right)^2+\left(e_5\omega\right)^2}, \tag{47}$$

$$\lambda_6=\sqrt{\left(k\omega\right)^2+\left(e_6\omega\right)^2}, \tag{48}$$

$$\lambda_7=\sqrt{\left(k\omega\right)^2+\left(e_7\omega\right)^2}, \tag{49}$$

$$\lambda_8=\sqrt{\left(k\omega\right)^2+\left(e_8\omega\right)^2}, \tag{50}$$

$$\lambda_0=\sqrt{\left(l\omega\right)^2+\left(k\omega\right)^2}. \tag{51}$$

The general solution of the equation is

$$Z_i\left(z\right)=K_{1i}e^{-\lambda_i z}+K_{3i}e^{\lambda_i z}\quad i=0,1,2,\ldots,8, \tag{52}$$

where K_{1i} and K_{3i} are constants. The boundary conditions (zero scalar potential for $z=\pm\infty$),

$$Z_{\psi 1i}\left(z\right)=K_{1i}e^{-\lambda_i z}\ \text{ for }\ i=0,1,2,\ldots,8 \tag{53}$$

$$Z_{\psi 3i}\left(z\right)=K_{3i}e^{\lambda_i z}\ \text{ for }\ i=0,1,2,\ldots,8. \tag{54}$$

In region 2, the equation is similar to equation (42) and replaces the 0 with the down side of equation (31). The solution is,

$$Z_i\left(z\right)=K_{2i}e^{-\lambda_i z}+T_{2i}e^{\lambda_i z}-\frac{MC}{\lambda_i^{\,2}\mu_r}g\left(k\right)e_i\omega \quad \text{for}\ \ i=1,2,3,4 \tag{55}$$

$$Z_j\left(z\right)=K_{2j}e^{-\lambda_j z}+T_{2j}e^{\lambda_j z}-\frac{MC}{\lambda_j^{\,2}\mu_r}g\left(l\right)e_j\omega, \quad \text{for}\ j=5,6,7,8 \tag{56}$$

$$Z_0\left(z\right)=K_{20}e^{-\lambda_0 z}+T_{20}e^{\lambda_0 z}, \tag{57}$$

where K_{2i}, T_{2i}, K_{2j}, T_{2j}, K_{20} and T_{20} are constants. The above constants can be calculated with the boundary conditions. The expression for the magnetic flux density in region 3 is,

$$\begin{aligned}B_{3x}=&-\sum_{k=1}^{\infty}\sum_{l=1}^{\infty}B_r k\omega K_{30}e^{\lambda_0 z}\cos\left(k\omega x\right)\sin\left(l\omega y\right)\\&-\sum_{k=1}^{\infty}\sum_{l=1}^{\infty}\sum_{u=1}^{\infty}B_r\sin\left(l\omega y\right)\sum_{i=1}^{4}K_{3i}e^{\lambda_i z}e_i\omega\cos\left(e_i\omega x\right)\\&-\sum_{k=1}^{\infty}\sum_{l=1}^{\infty}\sum_{u=1}^{\infty}B_r k\omega\cos\left(k\omega x\right)\sum_{j=5}^{8}K_{3j}e^{\lambda_j z}\sin\left(e_j\omega y\right)\end{aligned} \tag{58}$$

$$\begin{aligned}B_{3y}=&-\sum_{k=1}^{\infty}\sum_{l=1}^{\infty}B_r l\omega K_{30}e^{\lambda_0 z}\sin\left(k\omega x\right)\cos\left(l\omega y\right)\\&-\sum_{k=1}^{\infty}\sum_{l=1}^{\infty}\sum_{u=1}^{\infty}B_r l\omega\cos\left(l\omega y\right)\sum_{i=1}^{4}K_{3i}e^{\lambda_i z}\sin\left(e_i\omega x\right)-\\&\sum_{k=1}^{\infty}\sum_{l=1}^{\infty}\sum_{u=1}^{\infty}B_r\sin\left(k\omega x\right)\sum_{j=5}^{8}K_{3j}e_j\omega e^{\lambda_j z}\cos\left(e_j\omega y\right),\end{aligned} \tag{59}$$

$$B_{3z} = -\sum_{k=1}^{\infty}\sum_{l=1}^{\infty} B_r \lambda_0 K_{30} e^{\lambda_0 z} \sin(k\omega x)\sin(l\omega y)$$
$$-\sum_{k=1}^{\infty}\sum_{l=1}^{\infty}\sum_{u=1}^{\infty} B_r \sin(l\omega y)\sum_{i=1}^{4} \lambda_i K_{3i} e^{\lambda_i z} \sin(e_i \omega x) \quad (60)$$
$$-\sum_{k=1}^{\infty}\sum_{l=1}^{\infty}\sum_{u=1}^{\infty} B_r \sin(k\omega x)\sum_{j=5}^{8} \lambda_j K_{3j} e^{\lambda_j z} \sin(e_j \omega y),$$

where for $\mu_r = 1$, and

$$K_{3i} = \frac{Cg(k)e_i\omega}{2\lambda_i^2}\left(e^{-\lambda_i m_t} - e^{-\lambda_i m_b}\right) \quad i = 1,2,3,4 \quad (61)$$

$$K_{3j} = \frac{Cg(l)e_j\omega}{2\lambda_j^2}\left(e^{-\lambda_j m_t} - e^{-\lambda_j m_b}\right) \quad j = 5,6,7,8, \quad (62)$$

$$K_{30} = \frac{a_k a_l}{2\lambda_0}\left(e^{-\lambda_0 m_t} - e^{-\lambda_0 m_b}\right). \quad (63)$$

III. OPTIMIZATION OF THE NEW MAGNET ARRAY

Observing the magnet array proposed by this paper and the magnet array used by Jansen [4], the only difference is magnets of horizontally magnetized direction. Figure 5 shows the ratio between the higher harmonics and the analytical model in *z*-component of the magnetic flux density along the air gap length. The analytical model of the magnet array used in this paper is obtained by taking the first harmonic of the magnetic flux density and τ_m/τ takes 0.68 [4].

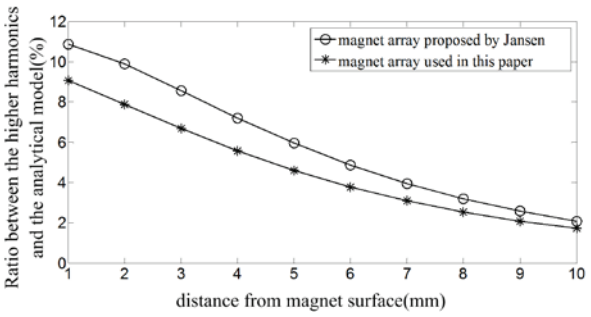

Fig. 5. Ratio between the higher harmonics and the analytical model in *z*-component of the magnetic flux density along the air-gap length.

The magnet array with hexagon magnets has lower ratio than the magnet array used by Jansen. The hexagon magnets can reduce the higher harmonics. The expressions of the magnetic flux density are too complicated to take the first harmonic of the *z*-component as the analytical model used in the real time control for planar motor. Then the effective amplitude is applied as an alternative method. The analytical model of this new 2-D Halbach array can be generalized as in [9],

$$B_{3eff}(\vec{x}) = e^{\sqrt{2}\omega z}\begin{bmatrix} B_{xy}\cos(\omega x)\sin(\omega y) \\ B_{xy}\sin(\omega x)\cos(\omega y) \\ B_z \sin(\omega x)\sin(\omega y) \end{bmatrix}, \quad (64)$$

where B_{xy} and B_z are the effective amplitudes of the magnetic flux density at z = -7.5 mm, and can be calculated as,

$$B_z = B_{3z}^{47}(0.5\tau, 0.5\tau, z_u) \Big/ e^{\sqrt{2}\omega z_u} \quad (65)$$

$$B_{xy} = B_z / \sqrt{2}. \quad (66)$$

The amplitude of *z*-component of the magnetic flux density can be predicted with equation (60) using Matlab. The maximum amplitude of the *z*-component of the harmonic at 4 mm below the bottom of the magnet array is less than 6×10^{-5} T when k = 1, l = 49, and u = 49, which is much less than geomagnetic field (about 6×10^{-5} T) [2]. So the harmonic components can be ignored in optimization if any one of the harmonic numbers (k, l, or u) is more than 47. The approximate expression of the *z*-component of the magnetic flux density is,

$$B_{3z}^{n} = -\sum_{k=1}^{n}\sum_{l=1}^{n} B_r \lambda_0 K_{30} e^{\lambda_0 z} \sin(k\omega x)\sin(l\omega y)$$
$$-\sum_{k=1}^{n}\sum_{l=1}^{n}\sum_{u=1}^{n} B_r \sin(l\omega y)\sum_{i=1}^{4} \lambda_i K_{3i} e^{\lambda_i z} \sin(e_i \omega x) \quad (67)$$
$$-\sum_{k=1}^{n}\sum_{l=1}^{n}\sum_{u=1}^{n} B_r \sin(k\omega x)\sum_{j=5}^{8} \lambda_j K_{3j} e^{\lambda_j z} \sin(e_j \omega y)$$

where n = 47. Both the width and length of the area are half pitch is chosen to be the objective region. This square area is placed in the 4 mm below the bottom of the array, and a 25 × 25 points matrix of the area is taken. The horizontal thrusts [6], which reflect the main performance of a planar motor are generated by *z*-component of the magnetic flux density. The minimization of higher harmonics of the *z*-component is the objective function obtained using equations (64) to (67),

$$f\left(\frac{\tau_m}{\tau}\right) = \left| \frac{\sum_{m=1}^{25}\sum_{n=1}^{25} B_{3zh}(S_{mn}) - \sum_{m=1}^{25}\sum_{n=1}^{25} B_{3zeff}(S_{mn})}{\sum_{m=1}^{25}\sum_{n=1}^{25} B_{3zeff}(S_{mn})} \right| \times 100\% \quad (68)$$

where $S_{mn} = (0.02m\tau, 0.02n\tau, -0.0075)$.

The genetic algorithm toolbox of Matlab is used. The optimization parameters and variables are shown in Tables I and II, respectively. The flowchart of the parameter optimizing procedure using genetic algorithm (GA) [13] is shown in Fig. 6. The stall generations are 100, and the others use the default setup.

Table I: Optimization parameters.

Parameters	**Symbol**	**Value**	**Unit**
Pole pitch	τ	0.025	m
Position of the top surface of the array	m_t	0.0035	m
Position of the bottom surface of the array	m_b	-0.0035	m
Remanence of the permanent magnets	B_r	1.24	T

Table II: Optimization variable.

Optimization variable	**Constrain**
τ_m/τ	[0,1]

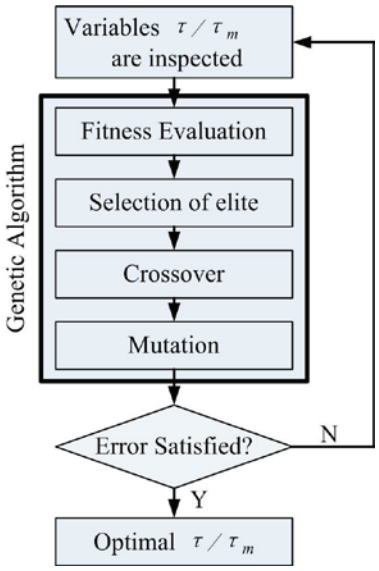

Fig. 6. The genetic algorithm process.

The fitness values of τ_m/τ shown in Fig. 7, illustrate that after 20 number of iteration the error reaches to an acceptable value. The minimization of the objective function can be obtained if τ_m/τ takes 0.41.

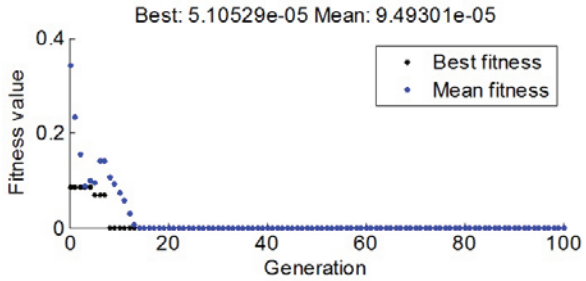

Fig. 7. Generation iteration process.

The magnetic flux density at 4 mm below the magnet array is shown in Fig. 8 when τ_m/τ takes 0.41. Figure 8 (a) is predicted with function shown in equation (61). Figure 8 (b) is calculated by 3-D finite-element model [13]. It can be found that Fig. 8 (b) approximates to Fig. 8 (a). The difference of the peak values between Fig. 8 (a) and Fig. 8 (b) is less than 0.01 T, which is 1.76 % of the peak value of Fig. 8 (a).

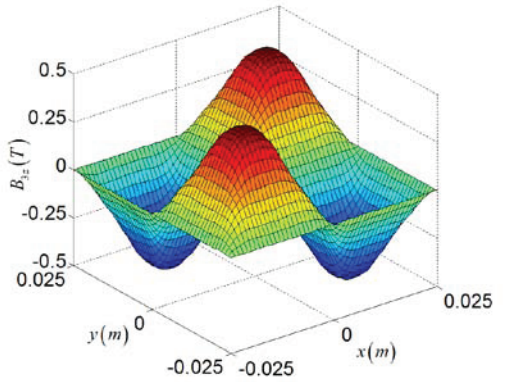

(a)

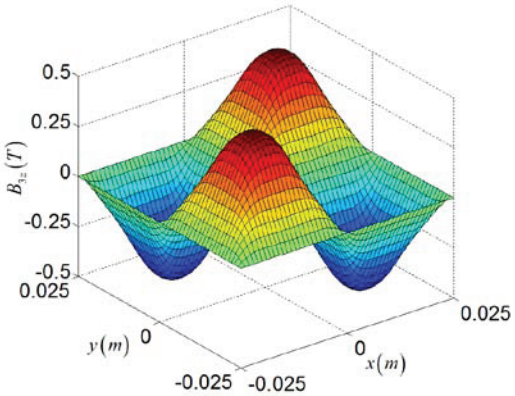

(b)

Fig. 8. Magnetic flux density, (a) calculated by the harmonic model and (b) calculated by the finite element method.

IV. SIMULATION AND COMPARISION

The Halbach array used by Jansen [4] has the same optimization parameters shown in Table I, and the results are shown with taking different optimization variable values in Table III.

Table III: Parameters compared.

Magnet array	τ_m/τ	$f(\tau_m/\tau)$
Proposed by this paper	0.41	0.0109%
Used by Jansen	0.68	6.277%

From Table III, the harmonic model is taken to obtain the sum for all the higher harmonics of z-component of the magnetic flux density on the plane, which is 4 mm below the magnet array surface. The sum of the magnet array proposed by this paper and used by Jansen is shown in Figs. 9 and 10, respectively.

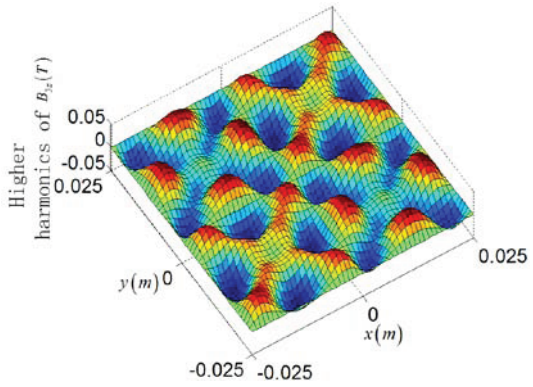

Fig. 9. The sum of all the higher harmonics components of the magnet array proposed by this paper.

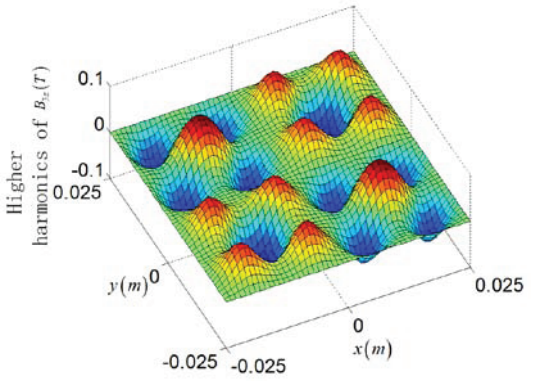

Fig. 10. The sum of all the higher harmonics components of the magnet array used by Jansen.

It is found that the sum for higher harmonics of z-component of the magnet array proposed by this paper is smaller and smoother than the magnet array used by Jansen. The peak value of higher harmonics of *z*-component of the magnet array proposed by this paper is 0.04097 T, which is 50.88 % of the peak value of the magnet array used by Jansen. If the magnet array proposed by this paper is used in the planar motor, the force ripple will be smaller than the planar motor in which the magnet array used by Jansen.

The peak value of *z*- and *x*-components of the magnetic flux density along the air-gap length from the magnet array surface are shown in Figs. 11 and 12, respectively. Comparing the curves in Figs. 11 and 12, the *z*-component of the magnetic flux density of the magnet array proposed by this paper is much larger than the magnet array used by Jansen, and the *x*-component of the magnetic flux density of the magnet array proposed by this paper is smaller.

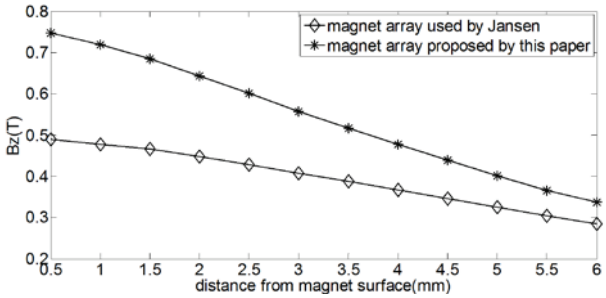

Fig. 11. Peak value of the *z*-component of the magnetic flux density along air-gap length.

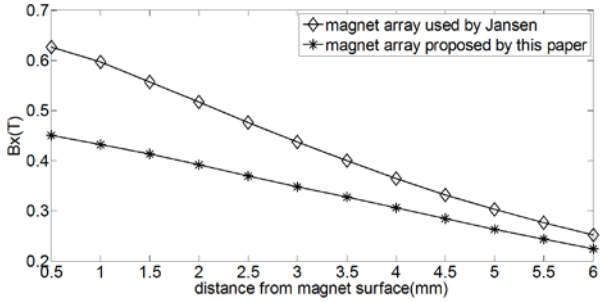

Fig. 12. Peak value of the *x*-component of the magnetic flux density along air-gap length.

V. CONCLUSION

The assumption of the air in the magnet array in the harmonic model derivation does not exist due to the compact structure. The hexagon

magnets can reduce the higher harmonics when compared with the magnet array used by Jansen. The analytical model is obtained by using the effective amplitude. The genetic algorithm is applied to minimize the higher harmonics of the *z*-component of the magnetic flux density of magnet array. Comparing with the magnet array used by Jansen, the higher harmonics of *z*-component of the magnetic flux density of this magnet array is much smaller, which will reduce the force ripple of the planar motor. The *z*-component of the magnetic flux density is larger and the *x*-component of the magnetic flux density is smaller.

ACKNOWLEDGMENT

Research was supported by National Natural Science Foundation of China (No. 51375194).

REFERENCES

[1] J. Compter, "Electro-dynamic planar motor," *Precision Eng.*, vol. 28, pp. 171-180, 2004.

[2] H.-S. Cho, C.-H. Im, and H.-K. Jung, "Magnetic field analysis of 2-D permanent magnet array for planar motor," *IEEE Trans. Magn.*, vol. 37, no. 5, Sep. 2001.

[3] H.-S. Cho and H.-K. Jung, "Analysis and design of synchronous per-manent-magnet planar motors," *IEEE Trans. Energy Convers.*, vol. 17, no. 4, pp. 492-499, Dec. 2002.

[4] J. Jansen, C. Van Lierop, E. Lomonova, and A. Vandenput, "Modeling of magnetically levitated planar actuators with moving magnets," *IEEE Trans. Magn.*, vol. 43, no. 1, pp. 15-25, Jan. 2007.

[5] J. Jansen, C. Van Lierop, E. Lomonova, and A. Van-Denput, "Magnetically levitated planar actuator with moving magnets," *in Proc. IEEE Int. Electric. Machines and Drives Conf.*, vol. 1, pp. 272-278, May 2007.

[6] W. Min, M. Zhang, Y. Zhu, B. Chen, G. Duan, J. Hu, and W. Yin, "Analysis and optimization of a new 2-D magnet array for planar motor," *IEEE Trans. Magn.*, vol. 46, no. 5, May 2010.

[7] Y. Zhang, Z. Yang, M. Yu, K. Lu, Y. Ye, and X. Liu, "Analysis and design of double-sided air core linear servo motor with trapezoidal permanent magnets," *IEEE Trans. Magn.*, vol. 47, no. 10, Oct. 2011.

[8] L. Huang, X. Huang, H. Jiang, and G. Zhou, "Comparative study of magnetic fields due to types of planar permanent magnet array," *International Conference on Electrical and Control Engineering*, vol. 10, 2010.

[9] J. Peng and Y. Zhou, "Modeling and Analysis of a new 2-D Halbach array for magnetically levitated planar motor," *IEEE Trans. Magn.*, vol. 49, no. 1, pp. 618-627, Jan. 2013.

[10] A. Shiri and A. Shoulaie, "Investigation of frequency effects on the performance of single-sided linear induction motor," *Applied Computational Electromagnetics Society (ACES) Journal*, vol. 27, no. 6, pp. 497-504, June 2012.

[11] K. Binns, P. Lawrenson, and C. Towbridge, *The Analytical and Numerical Solutions of Electrical and Magnetic Fields*, Chichester, England: *John Wiley & Sons*, 1994.

[12] A. Nejadpak, M. Barzegaran, and O. Mohammed, "Evaluation of high frequency electromagnetic behavior of planar inductor designs for resonant circuits in switching power converters," *Applied Computational Electromagnetics Society Journal*, vol. 26, no. 9, pp. 737-748, 2011.

[13] E. Schmidt and M. Hofer, "Application of the sliding surface method with 3D finite element analyses of a hybrid magnetic bearing," *25th Annual Review of Progress in Applied Computational Electromagnetics (ACES)*, pp. 440-445, Monterey, California, March 2009.

Guangdou Liu received the M.S. degree in Mechanical and Electronics Engineering from China University Of Petroleum, Shandong, China, in 2009, and is currently working toward the Ph.D. degree in Mechanical and Electronics engineering at the Huazhong University of Science Technology. His research interests include magnetic fields and magnetic devices.

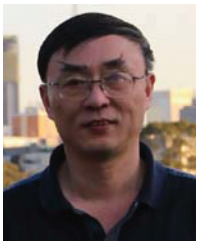

Yunfei Zhou received the B.S. degree in Mechanics from Zhejiang University, Hangzhou, China, in 1982, and the M.S. and Ph.D. degrees in Mechanical and Electronic Engineering from Huazhong University of Science and Technology, Wuhan, China, in 1989 and 1993, respectively. He is currently a Professor in Department of Mechanical and Electronic Engineering, Huazhong University of Science and Technology. His research interests include numerical control technology, high-precision motion control, microelectronic device, and precision servo motor control.